JOURNAL OF BIOMOLECULAR STRUCTURE AND DYNAMICS
https://doi.org/10.1080/07391102.2020.1796809

Antimalarial-agent artemisinin and derivatives portray more potent binding to Lys353 and Lys31-binding hotspots of SARS-CoV-2 spike protein than hydroxychloroquine: potential repurposing of artenimol for COVID-19

Moussa Sehailia and Smain Chemat

Research Centre in Physical and Chemical Analysis (C.R.A.P.C), Tipaza, Algeria

Communicated by Ramaswamy H. Sarma

ABSTRACT

Medicinal herbs have proved along history to be a source of multiple cures. In this paper, we demonstrate how hydroxychloroquine can act as a good inhibitor of SARS-CoV-2 Spike protein receptor-binding-domain using molecular docking studies. We also unveil how hydroxychloroquine can interfere in the prevention of Lys353 in hACE2 from interacting with the corresponding binding hotspot present on the Spike protein. Further screening of artemisinin & derived compounds produced better Vina docking score than hydroxychloroquine (-7.1 kcal mol^{-1} for artelinic acid vs. −5.5 kcal mol^{-1} for hydroxychloroquine). Artesunate, artemisinin and artenimol, showed two mode of interactions with Lys353 and Lys31 binding hotspots of the Spike protein. Molecular dynamics analysis confirmed that the formed complexes are able to interact and remain stable in the active site of their respective targets. Given that these molecules are effective antivirals with excellent safety track records in humans against various ailment, we recommend their potential repurposing for the treatment of SARS-CoV-2 patients after successful clinical studies. In addition, an extraction protocol for artemisinin from *Artemisia annua* L. is proposed in order to cope with the potential urgent global demand.

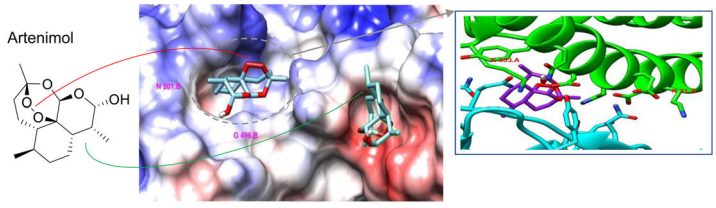

ARTICLE HISTORY
Received 21 April 2020
Accepted 6 July 2020

KEYWORDS
SARS-CoV-2; COVID-19; spike protein; hACE2; antiviral; hydroxychloroquine; artemisinin

HIGHLIGHTS

- Hydroxychloroquine role to prevent hACE2 from interacting with SARS-CoV-2 Spike protein is unveiled
- Artemisinin & derivatives entangle Lys353 & Lys31 binding hotspots of virus Spike protein and prevent infection
- Artemisinin, artesunate and artenimol stand as strong repurposing cadidates for COVID-19 clinical trials

Introduction

The spread of COVID-19 pandemic has triggered a race to unveil the secrets of severe SARS-CoV-2 and its underlying acute respiratory syndrome. Although, functional importance of different targets has been linked to the viral replication and maturation of coronaviruses' family such as Chymotrypsin-like protease(3CLpro) or known as Mpro (Khan et al., 2020; Muralidharan et al., 2020) or Envelope protein (E) (Gupta et al., 2020; Boopathi et al., 2020) but it has been confirmed that the binding of the viral trimeric surface spike glycoprotein (SProtein) of SARS-CoV-2 to the human receptor angiotensin-converting enzyme 2 (hACE2) is the first step in host infection (Zhou et al., 2020). In fact, Vankadari and Wilce (2020) revealed that S1 domains of the spike protein has an open conformation, enabling it to interact with target host proteins. Yan et al. (2020) identified the structure of hACE2 as a dimer in complex with membrane protein, they also showed that the two trimeric SProteins of the receptor

CONTACT Smain Chemat chemats@yahoo.fr Research Centre in Physical and Chemical Analysis (C.R.A.P.C), BP 384 Zone Industrielle de Bousmail, Tipaza CP42004, Algeria

Supplemental data for this article can be accessed online at https://doi.org/10.1080/07391102.2020.1796809.

binding domain (RBD) of SARS-CoV-2 bind very tightly to the hACE2 dimer. The latter is activated by a specific cellular enzyme called furin (Hasan et al., 2020).

Medicinal plants reap an important source of complex active molecules that have been proposed, and sometimes traditionally used for the treatment of several pathologies, such as cancer, autoimmune diseases, and infectious diseases. The scientific community are relying on different modes and various mechanisms of action these molecules hold to halt SARS-CoV-2 severity. Recently, remdesivir and chloroquine have been proved to inhibit *in vitro* Vero E6 cells of emerged novel coronavirus (2019-nCoV) (Wang et al., 2020). Chloroquine has been envisaged for SARS-CoV-1 (De Clercq, 2006), and has long been used for malaria therapy but has been replaced with hydroxychloroquine (HCQ) due to the increased *Plasmodium falciparium* parasite resistance, whereas an overdose of CQ can cause acute poisoning and death (Weniger, 1979). They have shown similar activities in *in-vivo* essays against malaria parasite but accompanied by an increased risk of retinopathy (Schrezenmeier & Dörner, 2020). Nonetheless, HCQ is considered safer than CQ as the later has mediated cardiotoxic effects including rhythm disorders, and propels the development of cardiomyopathy in patients with rheumatic diseases (Schrezenmeier & Dörner, 2020). For its turn, HCQ has been found to be effective in inhibiting SARS-CoV-2 infection *in vitro* and attenuate inflammatory response (Liu et al., 2020). Organic extracts of *Artemisia annua* L. have been found to be more effective, faster, and less toxic than CQ and HCQ in treating malaria. *A. annua* contains a vital compound known as artemisinin, a sesquiterpene lactone with a peroxide linkage exhibiting low toxicity (Table 1), also the parent compound for semisynthetic derivatives chemically modified at the C-10 position to produce artesunate, artemether, arteether, artenimol (dihydroartemisinin), and artelinic acid (Table 1). These compounds, and in some cases their sodium salts, have been formulated as antimalarials for oral, rectal, and parenteral administration (Woodrow et al., 2005).

Several reports proved the efficiency of artemisinin derivatives as potent antivirals for HPV bovine viral diarrhea virus (BVDV) for the treatment of anal and cervical intraepithelial high-grade neoplasia, human herpes virus-6 (HHV-6), human immunodeficiency virus (HIV) and more particularly, artesunate, against human cytomegalovirus (HCMV) (D'Alessandro et al., 2020). This antiviral potency put artemisinin class of compounds as promising candidates for the treatment of patients suffering from SARS-CoV-2 virus.

The encouraging results generated from the utilization of HCQ to treat patients suffering from COVID-19 pandemic further raises many questions surrounding its mode of action (Million et al., 2020). At the cellular level, direct and indirect mechanisms of CQ and HCQ are believed to inhibit immune activation by reducing Toll-like receptor signaling and cytokine production and, in T cells, reducing CD154 expression (Schrezenmeier & Dörner, 2020); however, the absence of binding assay studies between the SProtein and hACE2 protein in the presence of HCQ opens the door to two main possibilities (Vincent et al., 2005): the first possibility revolves around HCQ prevention of terminal glycosylation of hACE2 protein which consequently impacts the final attachment between the SProtein and hACE2 protein, whereas the second possibility revolves around HCQ interaction with the receptor binding domain (RBD) of SProtein, thus preventing its docking on hACE2 receptor.

To further expand on the second possibility, we elected to perform computational studies based on molecular docking to help us understand more about the mode of interaction between HCQ and the RBD of SARS-CoV-2 SProtein, and eventually, how such interaction prevents the SProtein from docking on the hACE2. Another class of antimalarial and antiviral molecules comprised of artemisinin and artemisinin derived compounds are investigated to reveal how effective these molecules act with binding sites of SProtein, then ultimately how their mode of interaction occur.

This study aims to propose also an extraction protocol for artemisinin from *Artemesia annua* L. in order to cope with the potential urgent global demand.

Material and methods

Molecular docking

The PDB file of SARS-CoV-2 SProtein RBD-hACE2 complex (PDB Ref. 6LZG, version 1.0) was obtained from the Research Collaboratory for Structural Bioinformatics (RCSB) protein data bank (PDB) (http://www.rcsb.org/structure/6LZG). UCSF Chimera1.14 was used to visualise the structure of the ligand and/or protein-complex structure, to perform the various functions associated with ligand and protein preparations, and acting as an interface to enable molecular docking calculations using locally hosted AutoDock Vina software (Pettersen et al., 2004; Trott & Olson, 2010). Prior to molecular docking, the hACE2 protein (part A, protein section coloured in Green-Figure 2) was deleted from the PDB file of the complex. In addition, all non-standard residues including that of water were also removed. The structure of each ligand was incorporated into UCSF Chimera using SMILES string followed by structure minimisation.

The PDBQT files of the SProtein RBD and each ligand was generated after adding all hydrogens and charges to each structure. The number of binding modes was set to 10 with exhaustiveness of search set to 8. The maximum energy difference was set to 3 kcal mol^{-1}. The best scoring pose for each molecule was analysed in terms of its interaction with the receptor binding motif (RBM). The X, Y, Z coordinates of the grid box covered the full area of the receptor binding motif of the SProtein, in our case, for Center (X = −40.34, $Y = 27.28$, Z = −7.72) whereas for Size ($X = 24.05$, $Y = 51.38$, $Z = 21.79$). In the case of the receptor, all hydrogen atoms were added to the structure, charges were merged and non-polar hydrogen were removed; water molecules and side chains of non-standard residues were also ignored. For the studied ligands, charges were merged and non-polar hydrogens were also removed. The obtained molecular docking results were then aligned with the PDBQT file of the SProtein RBD-hACE2 complex in order to visualise the type of

Table 1. Top Vina score of artemisinin and its derivative compounds against SProtein RBM. (Highlighted in light-grey are compounds with good clinical records).

Entry	Name	Structure	Interacting residues*	Vina Score (kcal.mol^{-1})	Calculated Ki (μM)
1	Artelinic acid		H-bond: Ser494 vdW: Tyr505, Asn501, Gly496, Ser494, Gln493, Tyr453, Tyr495, Phe497	−7.1	6.16
2	Artesunate		H-bond: Gly496, Ser494 vdW: Gln493, Tyr495, Gln409, Ser494, Arg408, Glu406, Asp405	−6.8	10.23
3	Artemisone		H-bond: Gln498, Asn501, Gly496 vdW: Ser494, Tyr495, Tyr505, Tyr453, Gln493	−6.6	14.34
4	Artemisinin		H-bond: none vdW: Ser494, Gly496, Asn501, Tyr453, Gln493	−6.5	16.98
5	Artemiside		H-bond: none vdW: Gln493, Tyr453, Gly496, Asn501, Tyr505, Tyr495, Phe497,Ser494	−6.4	20.11
6	Artenimol (Dihydroartemisinin)		H-bond: none vdW: Tyr495, Gly496, Asn501, Tyr505, Phe497, Tyr453, Gln493, Ser494, Gln498	−6.4	20.11
7	Artemotil		H-bond: none vdW: Gly496, Tyr449, Gln498, Asn501, Tyr505, Phe497, Tyr453, Gln493, Ser494	−6.3	23.82
8	PubChem CID: 90667934		H-bond: none vdW: Tyr495, Gly496, Asn501, Tyr505, Phe497, Tyr453, Gln493, Ser494	−6.3	23.82
9	PubChem CID: 122185220		H-bond: Gln498, Tyr449 vdW: Tyr495, Asn501, Tyr505, Tyr453, Gln493, Ser494,, Phe497, Gly447	−6.3	23.82
10	Artemether		H-bond: none vdW: Tyr495, Gly496, Asn501, Tyr505, Arg403, Tyr453, Gln493,	−6.0	39.54
11	PubChem CID: 10380074		H-bond: Tyr453 vdW: Gly496, Tyr495, Tyr505, Arg403, Ser494	−6.0	39.54
12	HCQ		H-bond: Asn501, Gly496 vdW: Phe497, Gln498, Tyr505, Glu406, Tyr453, Ser494	−5.5	92.04

*refer to Figure 1S (Supplementary Information) for more information.
vdW: van der Waals forces.

interactions of each docked molecule in the SProtein-hACE2 binding interface.

Molecular dynamics

Computations were performed at the Al-Farabi Cluster computer of the Ecole Nationale Polytechnique Oran – Maurice Audin (Algeria). All molecular dynamics (MD) studies are performed using GROningen MAchine for Chemical Simulations (GROMACS) which is a software package designed to perform MD simulations of proteins, lipids and nucleic acids. Amber force field was utilised during the parameterisation of each protein complex system followed by solvation with TIP3P water molecules; water.tip3p force field in a cubic periodic box with 10 Å spacing protein-box edge was applied. Na + ions were introduced to neutralise the overall charge. Further energy minimisation was performed using steepest descent and conjugate gradient algorithms. The system was subjected to 100 ns MD at 300 K and pressure of 1 bar, the latter value was maintained using Berendsen barostat. The generated trajectory files were analysed using visual molecular dynamics (VMD) software.

Results and discussion

Most explanations associated with HCQ mode of action are based on findings revolving around the mode of action of CQ on SARS-CoV infection (Simmons et al., 2004; Yang et al., 2004). Amongst the cited reasons are: (i) CQ can increase the value of endosomal pH which can reduce the transduction

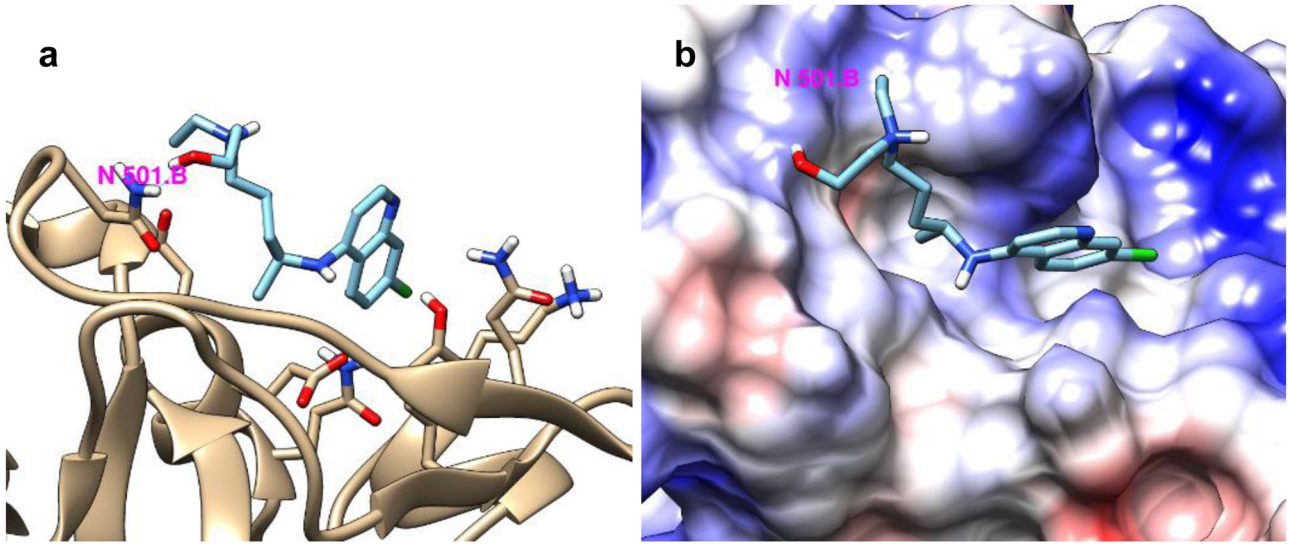

Figure 1. Top Vina pose of HCQ on SProtein RBM following molecular docking. (a) secondary structure of part of SProtein RBM bound to HCQ (hydrogen bond between Asn501 and OH group of HCQ is shown in blue line). (b) Columbic surface characteristics of the corresponding SProtein RBM bound to HCQ.

of SARS-CoV pseudo-type viruses (Simmons et al., 2004; Yang et al., 2004), (ii) CQ can raise the possibility of affecting the endosome-mediated fusion if added at the initial stage of the infection (Vincent et al., 2005), and (iii) once the virus is inside the cell, CQ can inhibit the production of glycoproteins in vesicular stomatitis, thus preventing virus replication (Dille & Johnson, 1982).

Previously, Vincent et al. (2005) showed that introduction of CQ prevents terminal glycosylation of ACE2 receptor protein of the host cell, thus destabilizing the recognition mode of the SProtein on the surface of the virus, albeit such action did not impact the level of expression of surface hACE2 proteins of the host cell. Therefore, we elected to perform computational docking studies of HCQ as safe CQ substitute against SProtein RBD of SARS-CoV-2 to further study the nature of such interaction and explore its inhibition potential against SProtein.

Molecular docking studies

Our molecular docking studies of HCQ on the RBD of SARS-CoV-2 SProtein produced a Vina score of -5.5 kcal mol^{-1} (Table 1). The obtained scoring is relatively moderate given that Vina score of the best molecule, i.e. Physalin b, previously docked on a homology model of SARS-CoV-2 SProtein RBD was -7.2 kcal mol^{-1} (Micholas & Jeremy, 2020). Analysis of our docking results showed that the hydroxyl group (OH) of HCQ molecule formed strong hydrogen bonding with Asn501 side chain residing on one part of the receptor binding motif (RBM) of the SProtein (Figure 1).

In the SPrtoein-hACE2 complex, Asn501 of SARS-CoV-2 Sprotein forms favourable hydrogen bonding with Tyr41 of hACE2 while at the same time helps neutralising the charge of Lys353 (Lan et al., 2020). Therefore, the resulting hydrogen bonding between the OH group of HCQ and Asn501 can play a role in destabilising other interactions with hACE2 residues, e.g. Tyr41, Lys353, Gly354 and Asp355, which were already found to play key roles in the interaction with the SProtein (Lan et al., 2020; Micholas & Jeremy, 2020; Yan et al., 2020).

Furthermore, when our initial docking results were aligned with the structure of SProtein-hACE2 complex, we successfully observed significant clash between the amino-alkyl side-chain of HCQ and the Lys353 residue side-chain of hACE2 (Figure 2). Equally, Lys353(O) was found to form one hydrogen bonding with Gln502 of the SProtein in the complex as reported by Lan et al. (2020); at the same time, Lys353(N) forms important hydrogen bonding with Gln496 while maintaining a salt bridge with Asp38 (Lan et al., 2020; Yan et al., 2020). Similar to Lan et al. (2020) findings, Lys353 and Lys31 were both found to be important hotpots in hACE2 responsible for binding to the SProtein of SAR-CoV-2. It is believed that the latter specie developed key mutations to help stabilise and/or neutralise both lysine hotspots via introduction of Asn501 (to neutralise Lys353) and Gln 493 & Leu 455 (to neutralise Lys31) of hACE2 protein, thus ensuring tighter incorporation of both hotspots deep into the hydrophobic pockets of the SProtein, which would explain the main reason behind the higher affinity of SARS-CoV-2 Sprotein to hACE2 compared to that of SARS-CoV (Lan et al., 2020). Therefore, it is very likely that selective interaction of HCQ with the surface of SARS-CoV-2 SProtein through the formation of an inclined tape over the hydrophobic pocket responsible for hosting the Lys353 hotspot (the OH group in this case is acting like a hook by forming a hydrogen bond with Asn501), can be responsible for the prevention of tighter binding with hACE2 protein *via* restricting penetration of Lys353 into its finally assigned destination on the SProtein RBD (Figure 2).

Similar to Asn501 in SARS-CoV-2, Thr487 in SARS-CoV SProtein was previously reported by Shang et al. (2020) to interact with Tyr41, Lys353, Gly354 and Asp355 in hACE2 protein. We advocate here that similarity in the hydrogen bond networking system between both types of SProteins (i.e. that of SARS-CoV and SARS-CoV-2) and that of hACE2 may be used to explain the supposed efficacy of HCQ in inhibiting SARS-CoV and SARS-CoV-2 interaction with hACE2. On the other hand, our molecular docking results also showed good interaction between the quinoline aromatic

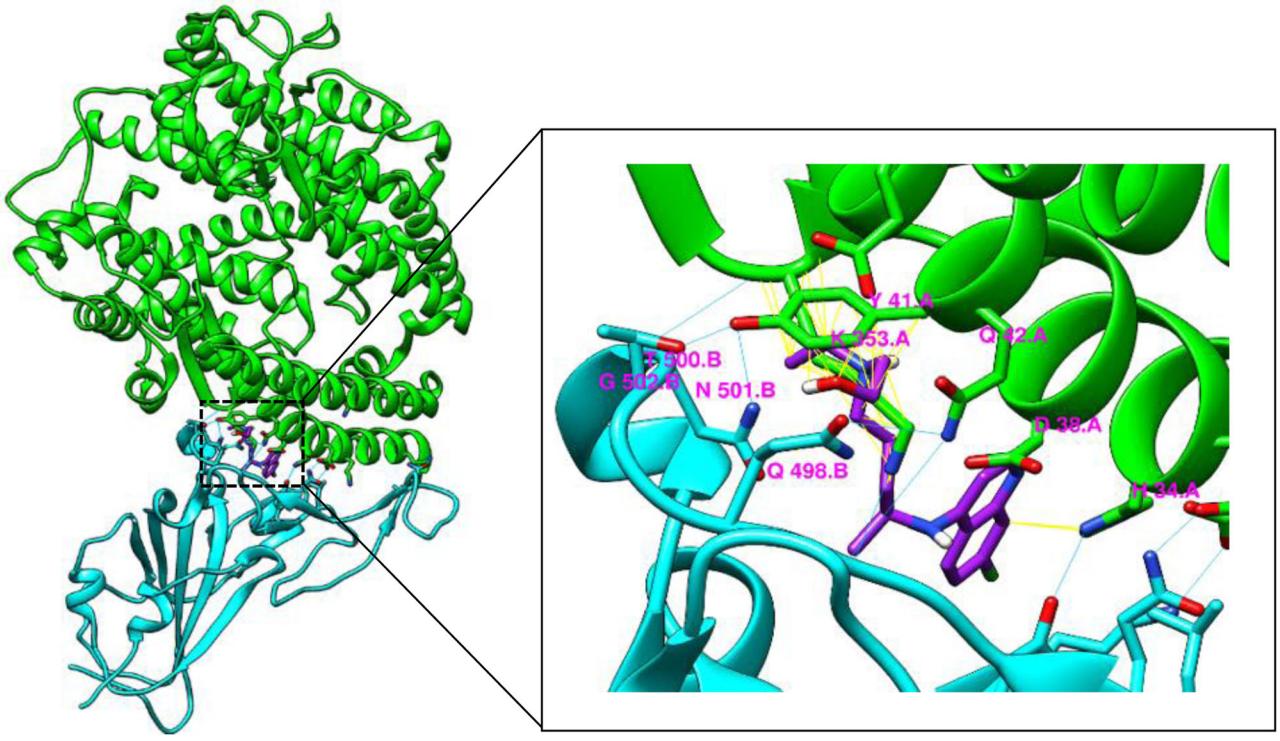

Figure 2. Alignment of HCQ top Vina pose with SProtein RBD-hACE2 complex structure. Hydrogen bondings are shown in blue lines. Clashes/contacts are shown in yellow lines. Direct clash is observed between the aminoalkyl chain of HCQ and the Lys353 side-chain. The secondary structure of SProtein RBD is shown in cyan whereas that of hACE2 is shown in green. HCQ is shown in purple.

ring in HCQ and His34 in hACE2; in normal circumstances, the latter residue interacts well with Leu455 and Gln493 of the SProtein. By doing that, HCQ can also disturb interaction in the middle region of the binding interface between the SProtein and hACE2 (Figure 2). Previously, Samarth and Kirk (2020) studied the interaction of hydroxychloroquine/azithromycin with SARS-CoV-2 SProtein-hAce2 complex using a virtualised quantum mechanical modelling approach. In agreement with our study, the authors found that HCQ had low potency of interaction with the studied complex compared to azithromycin; they also recommended molecular docking studies to further strengthen their rationale.

Our approach to study the interaction of molecules with the receptor binding motif (RBM) of the SProtein prior to complexation with hACE2 has helped properly analyse the type of interaction with the Sprotein, and how such interaction could prevent hACE2 from docking onto the RBM of SProtein. In addition, we successfully addressed some of the aspects surrounding the mechanism of action of HCQ and artemisinin derivatives in preventing the interaction between the virus' SProtein and hACE2 receptor via selectively interacting with the Lys353 binding hotspot of SProtein. With this information on hand, we then elected to perform *in-silico* screening of other potent antimalarial compounds derived from the core structure of artemisinin; by doing so, we believe we can gain more insight about the potential use of such class of compounds as safer and more potent substitutes to HCQ. In this regard, a total number of 11 compounds were successfully screened against SProtein RBD using the same molecular docking approach previously followed with HCQ. The obtained results are shown in Table 1.

Analyses of the data show that artemisinin and its derivative compounds have scored better than HCQ, with compounds in Entry 10 & 11 of Table 1 producing the least and closest Vina score (-6.0 kcal mol^{-1}) to HCQ. On the other hand, artelinic acid (Table 1, Entry 1) gave the best Vina score of -7.1 kcal mol^{-1}; however, this compound was discarded due to its high toxicity levels (Li et al., 2007). Although artemisinin and its derivative compounds resulted in good Vina scoring ($-6.0 \leq$ Score $\leq$ 7.1 kcal mol^{-1}), only those approved and prescribed as antimalarials were selected namely, artesunate (Table 1, Entry 2), artemisinin (Table 1, Entry 4) and artenimol (Table 1, Entry 6). These were found to possess good clinical records with very promising antiviral properties, thus enhancing their potential to be repurposed for the treatments of SARS-CoV-2. Artesunate (Table 1, Entry 2) with Vina score of -6.8 kcal mol^{-1}.

The calculated inhibition constant (Ki) of each top scoring pose is also reported in Table 1. Analysis of the data shows that artemisinin class of compounds possess much lower Ki than HCQ, thus enabling them to become good antiviral candidates against SARS-CoV-2. The elevated Ki value of HCQ also reflects the high cytotoxic concentration of HCQ (CC_{50} $>$ 100 μM at multiplicity of infection (MOI) $=$ 0.05) required to eradicate the virus during in-vitro assay studies as previously reported by Liu et al. (2020). Besides its antiviral activity, artemisinin derivatives hold immunoregulatory properties and modulate neutrophils, T-cell and B-cell components of the immune system (Yao et al., 2016), thus enhancing system immunity and touting themselves as promising candidates to synergistically enhance their antiviral effect in vivo and treat inflammation-associated diseases (Li et al., 2007). The nature

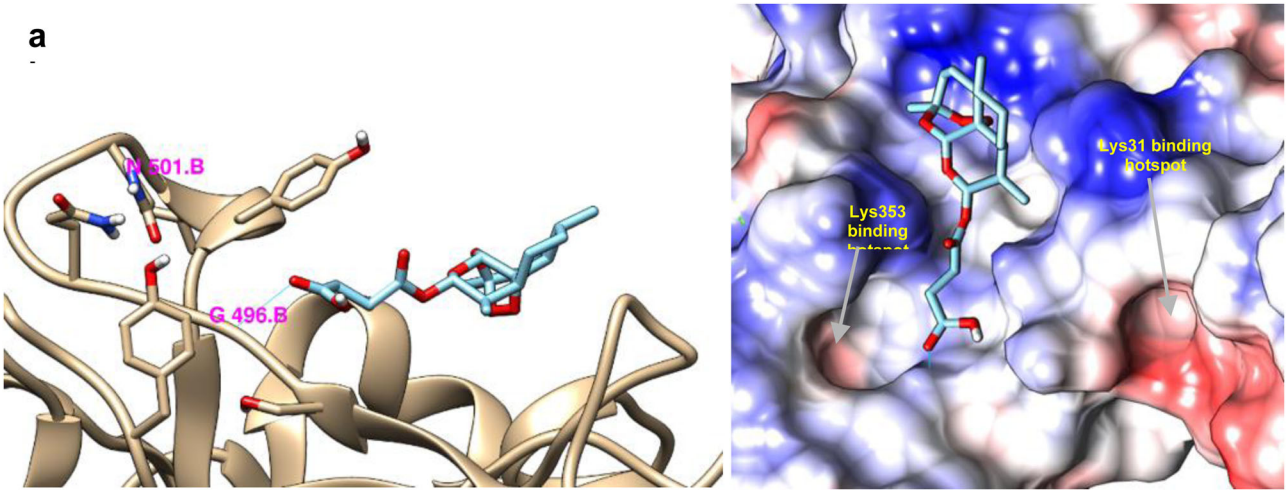

Figure 3. Top Vina pose of artesunate on SProtein RBM following molecular docking. (a) secondary structure of part of SProtein RBM bound to artesunate (hydrogen bond between Gln496 and carboxylic acid group of artesunate is shown in blue line). (b) Coulombic surface characteristics of the corresponding SProtein RBM bound to artesunate.

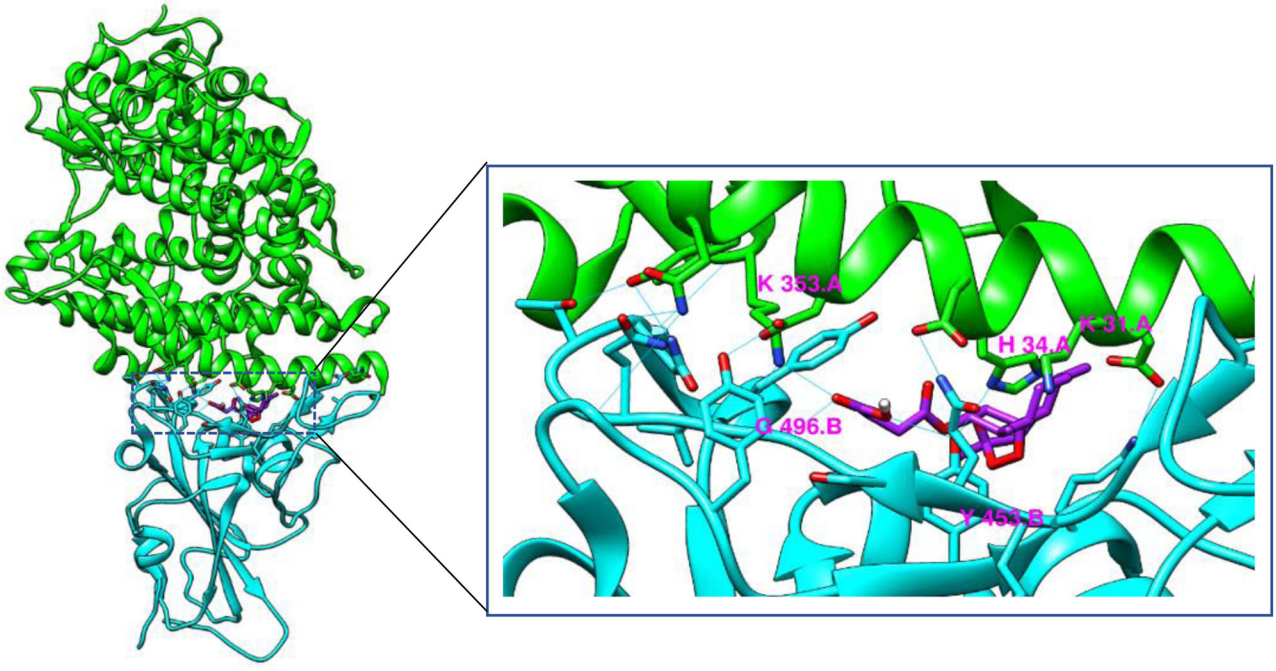

Figure 4. Top Vina scoring pose of artesunate aligned in the binding interface of SProtein RBD-hACE2 complex. Shown in cyan is the SProtein RBD whereas that in green show hACE2. Artesunate is shown in purple.

of interaction between the aforementioned three compounds and the RBD of SARS-CoV-2 SProtein was also analysed in order to see which molecule best influence the repulsion of hACE2 Lys353 and Lys31 from binding to the inner hydrophobic pockets of the SProtein. By analysing the top scoring pose of artesunate (Table 1, Entry 2), we observe that the molecule binds far away from the hydrophobic regions of Lys353 and Lys31 hotspot binding sites (Figure 3).

Furthermore, upon alignment of artesunate docking results with the structure of SProtein hACE2 complex, no clashes were observed between artesunate structure and the other side-chains present in the hACE2 protein. However, the carboxylic acid moiety of the artesunate side chain was observed to form hydrogen bonding with Lys353(N), which can further neutralise the overall charge through the formation of a salt bridge, this can adversely lead to tighter interaction between hACE2 and SProtein. Therefore, in spite of the high Vina scoring associated with artesunate, we predict that this molecule is unlikely to act as a good inhibitor, in its current form, to SARS-CoV-2 SProtein (Figure 4).

In the case of artemisinin's (Table 1, Entry 4) top pose, despite no hydrogen bonding is observed with the SProtein RBD, we notice a lateral incorporation of the six-membered ring cyclohexane group of artemisinin into the Lys353 hotspot binding pocket, with the peroxy-bridge facing the peripheral hydrophilic surface of the binding region(Figure 5 (a), region coloured in blue next to the peroxy-bridge). Such mode of interaction could well be used to prevent the penetration of Lys353 side-chain into the hydrophobic pocket (Figure 5). Artemisinin lateral penetration into these binding

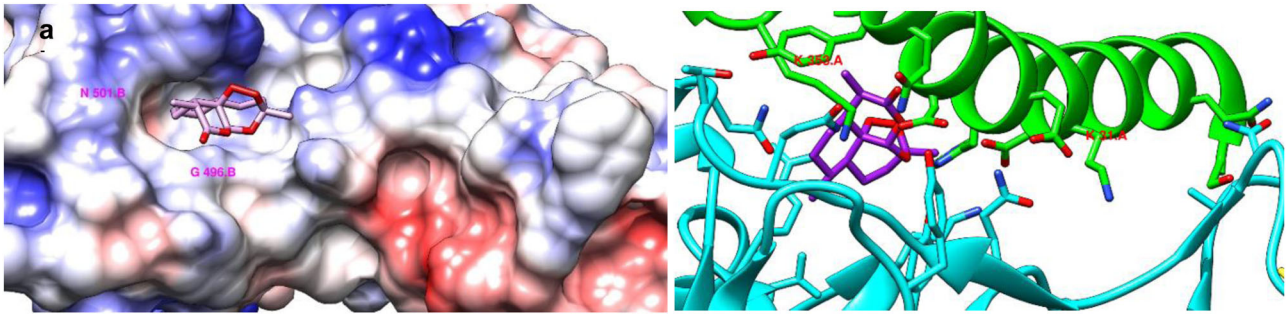

Figure 5. Top Vina pose of artemisinin on SProtein RBM (Lys353 binding hotspot) following molecular docking. (a) Columbic surface characteristics of part of the SProtein RBM bound to artemisinin. (b) Secondary structure of part of SProtein RBM bound to artemisinin.

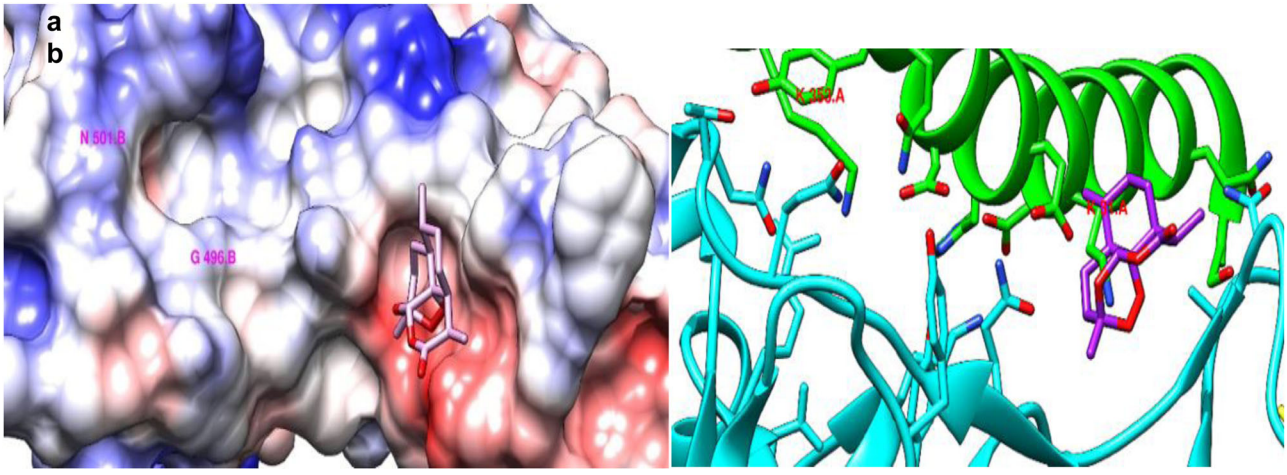

Figure 6. Vina pose of artemisinin on SProtein RBM (Lys31 binding hotspot) following molecular docking. (a) Columbic surface characteristics of part of the SProtein RBM bound to artemisinin. (b) Secondary structure of part of SProtein RBM bound to artemisinin.

hotspots may reduce the random motion of α-helix and loops present in SProtein and its capability to attach with hAC2 as hypothesized by Gupta et al. (2020) where binding with phytochemicals reduces their motion present in the Envelope (E) protein of SARS-CoV2, therefore inhibiting a modulation of ion channel activity and stop the pathogenesis caused via SARS-CoV2.

Artemisinin was also found to interact with Lys31 hotspot binding pocket, although at slightly lower Vina score (-5.6 kcal mol^{-1}). The average score is perhaps attributed to the absence of hydrophilic surfaces close to the binding pocket (Figure 6). Therefore, the selective interaction of artemisinin with both Lys353 and Lys31 hotspot binding regions raises its possibility to be repurposed for the treatment of SARS-CoV-2 patients following successful clinical trials. Artemisinin has better tolerance on human hepatoma cell line HepG2 with CC50 of 160 mM than artesunate CC50 of 20 mM (Romero et al., 2005). Additionally, *in vitro* cytoxicity levels of artesunate against human epithelial cells (HeLa cells) and human foreskin fibroblasts (HFF cells) report very low tolerance with CC50 of 71.7 mM and 7.1 mM respectively (He et al., 2013).

Artenimol on the other hand showed a similar mode of interaction to that of artemisinin with both Lys353 and Lys31 hotspot binding sites, although at slightly lower Vina scores of −6.4 and −5.4 kcal mol^{-1}, respectively (Figure 7). Both artemisinin and artesunate are susceptible to CYP450 reduction to generate artenimol once incorporated into the human body, albeit at different conversion rates. We therefore recommend that artenimol can be prioritised for clinical trials to achieve the repurposing of such class of molecules for COVID-19, however, careful considerations need to be taken into account given the water solubility characteristics of each compound (Woodrow et al., 2005).

Molecular dynamics analysis

Successful completion of MD calculations permitted us to obtain two crucial graphs, i.e. that of root-mean square deviation (RMSD) vs. time (Figure 8) and the root-mean square fluctuation (RMSF) of each residue in the three protein complexes, i.e. that of the SProtein RBM in complexation with HCQ, artemisinin or artenimol (Figure 9).

RMSD represents a measure of the average change in the displacement of an atom for a particular frame compared to a reference frame. On the other hand, RMSF measures the local changes of each residue in the protein backbone. Figure 8 indicates a good protein-ligand stability for all three complexes, with HCQ protein complex showing the lowest RMSD value (0.22 Å) followed by artenimol-protein complex (0.24 Å) and artemisinin-protein complex (0.26 Å). Similarly, artemisinin-protein complex showed the highest deviation 0.4 Å followed by artenimol-protein complex 0.37 Å and HCQ-protein complex 0.34 Å. Those values imply the

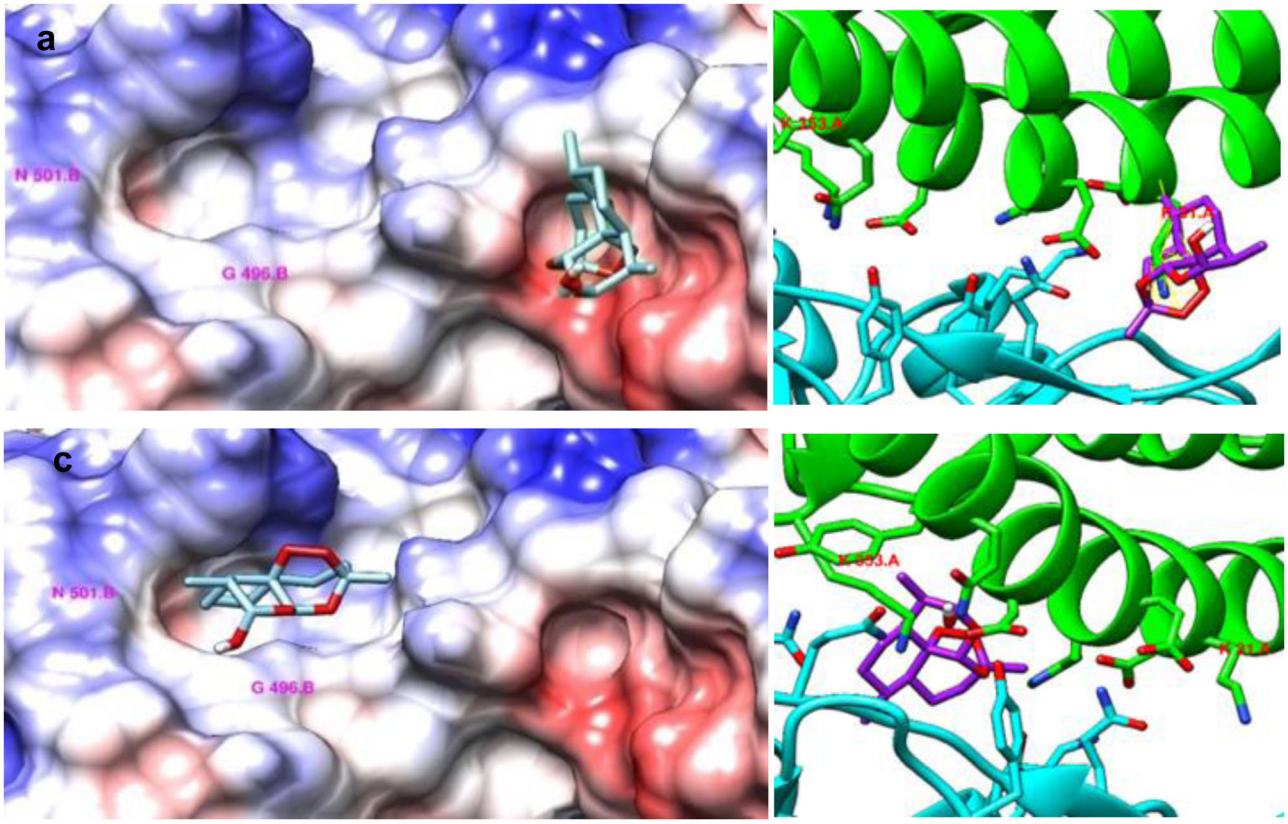

Figure 7. Top Vina pose of artenimol on SProtein RBM (Lys353 & Lys 31 binding hotspot) following molecular docking. (a) Columbic surface characteristics of part of the SProtein RBM bound to artenimol in the Lys31 binding hotspot. (b) Secondary structure of part of SProtein RBM bound to artenimol in the Lys31 binding hotspot. (c) Columbic surface characteristics of part of the SProtein RBM bound to artenimol in the Lys353 binding hotspot. (d) Secondary structure of part of SProtein RBM bound to artenimol in the Lys353 binding hotspot.

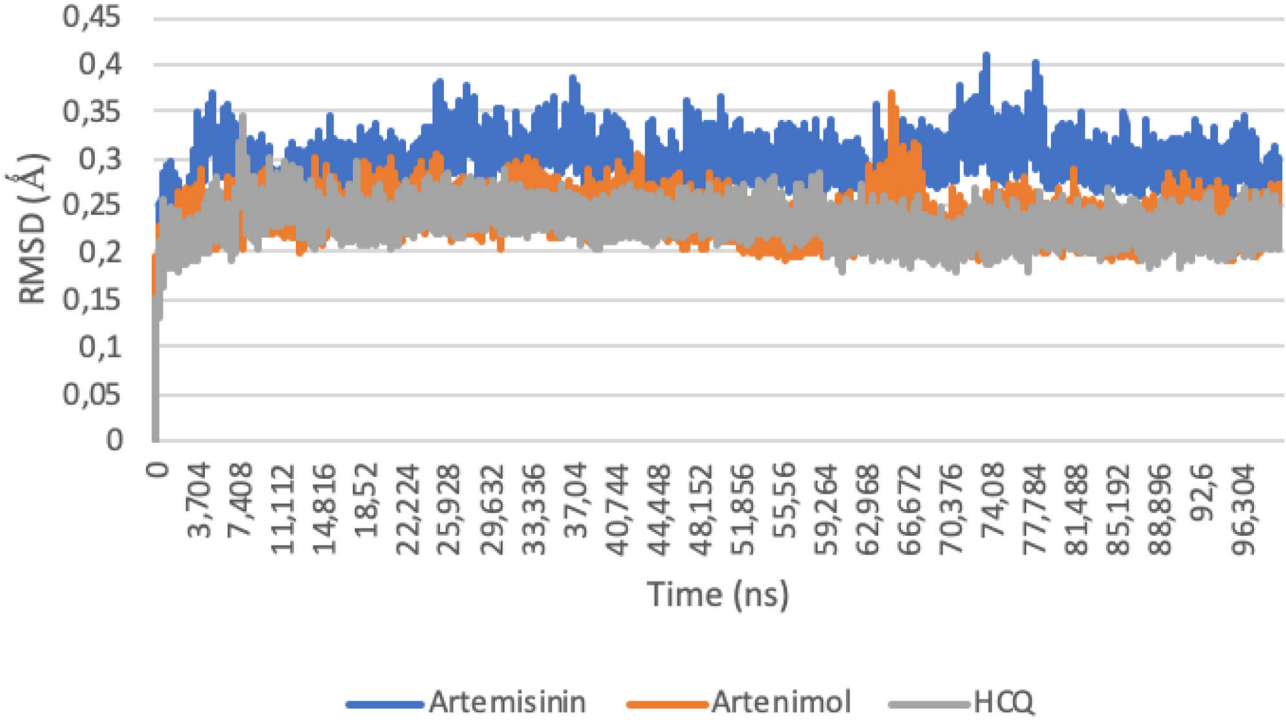

Figure 8. RMSD vs time for three ligand-protein complexes.

presence of a much stable protein backbone for the three protein complexes. The RMSF graph demonstrated a similar trend of fluctuation for all three ligand-protein complexes; major fluctuations are noted at the terminal residues of the protein backbone (353 & 527), with HCQ-protein complex showing highest fluctuation at residue 527 (5.5 Å) followed

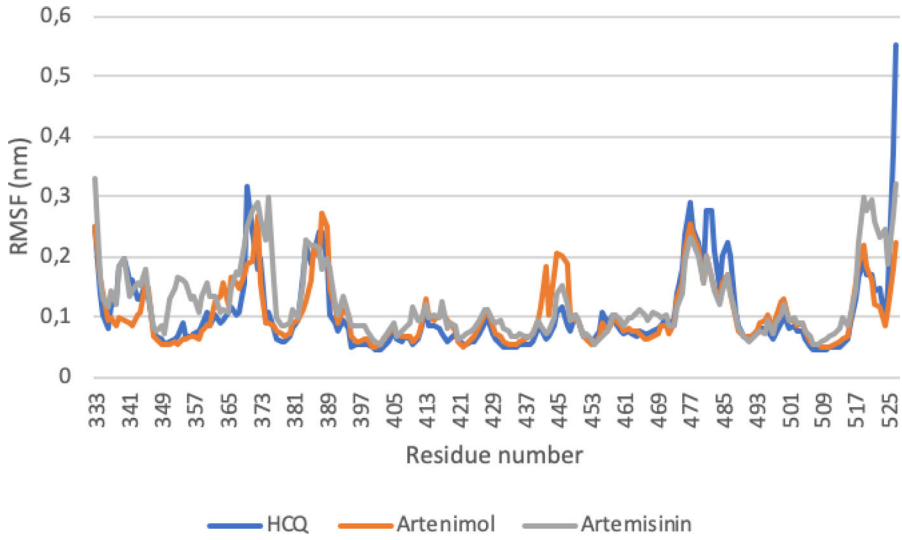

Figure 9. RMSF vs. residue number for each ligand-protein complex.

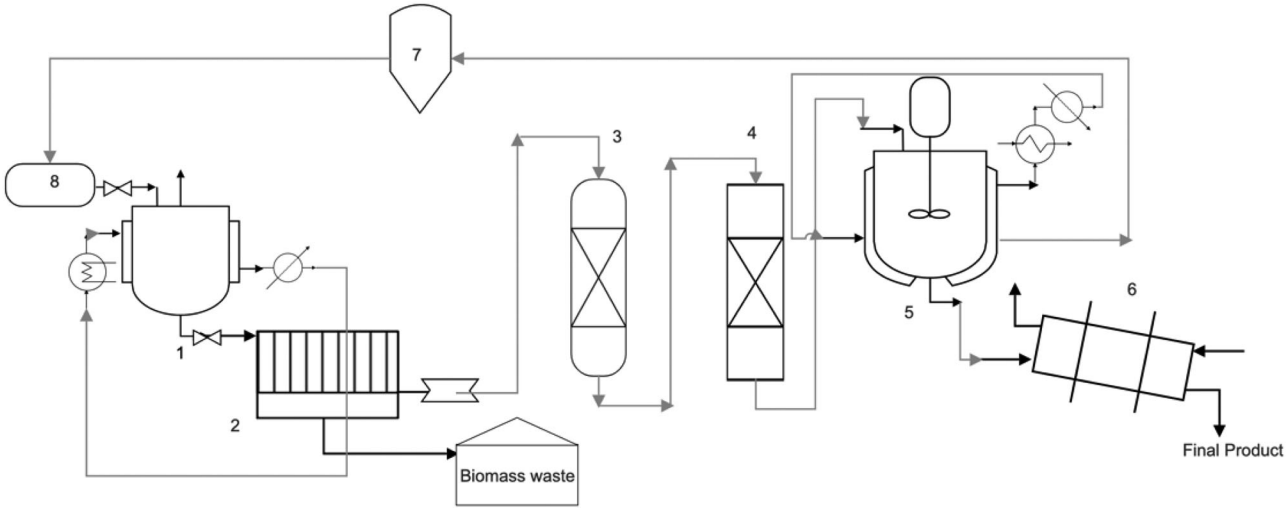

Figure 10. Simplified extraction plant for high purity Artemisinin.
1: Extraction reactor; 2: Frame and plate filter-press (or vibrating-screener/decanter); 3: Adsorption column bed; 4: Clarification column bed; 5: Crystallization stirred reactor; 6: Spray dryer; 7: Distillation column; 8: Solvent storage tank

by artemisinin (3.1 Å) and artenimol (2.2 Å). Other areas of fluctuations (1.4 < RMSF < 3.0) include residues at (477-485), (444-447), (383-389), (369-373). Overall, low fluctuations during long trajectory were observed throughout the protein backbone of each ligand-protein complex which indicate their ability to remain stable at the active site of their targets. This result is similar to Ramos et al. (2019) findings of potential inhibitors of the enzyme acetylcholinesterase and juvenile hormone with subsequent long-trajectory MD indicating a considerable stability of the novel molecules.

Proposed artemisinin extraction process

Currently, major production of artemisinin is based on solvent extraction from *A. annua* despite modest but not scalable enough trials to produce it chemically or semi-synthetically via its precursor artemisinic acid in engineered bacteria (Hale et al., 2007; Dietrich et al., 2009). Artemisinin is abundant in *A. annua* leaves (0.4-1.4%) and production includes several steps starting with screening and drying before biomass being processed generally via solvent leaching or percolation at 30-50 °C using low polarity solvents like hexane, toluene or petroleum (Chemat et al., 2019). This operation is not selective for artemisinin, therefore terpenes, fatty acids and some pigments are inevitably co-extracted which calls for secondary refinery steps including adsorption, flash chromatography and sequential crystallization. Herein, an indicative facile production setup is proposed to enhance worldwide production capacity (Figure 10). However, a fire-proof equipment and facility is a pre-requisite to ensure safety and security measures are met.

The plant comprises an extraction step (1) in which biomass is placed in hollow-fibre bags and processed at 40 °C for 60 min using a solvent mixture of hexane/ethyl acetate (95:5 v/v) with solvent/biomass ratio of 6 to 1 (6 L for each Kg) (Chemat et al., 2017). This step can be conducted by means of a stirring tank or a percolation type reactor to

ensure up to 99% extraction yield is achieved. Then, the mixture passes through a cloth or diaphragm plate and frame filter-press (2) in order to discard fine biomass particles and recover the extract. The latter is submitted to an adsorption bed column (3) filled with activated carbon aiming at the removal of pigments and tannins. Another clarification stage is required to remove other impurities such as free fatty acids and pigments; for instance, an adsorption bed column (4) filled with Celite 545 (Merck) is recommended (Chemat et al., 2017). Due to some affinity with activated carbon and Celite 545, an artemisinin loss of 3-5% is expected.

After that, the purified extract should be concentrated to at least 1/8th its initial volume using an evaporator. The concentrated extract is submitted into a jacketed crystallization reactor (6) equipped with a stirring shaft set at tip-speed in the range of 100-150 rpm to control breakage effects and to generate a narrow particle size distribution (Huter et al., 2018). The cooling rate is set to 0.5 °C/min to reach 4 °C and is kept at this temperature for 60 min to let artemisinin crystals settle down. The crystals are sent into a spray drying system (7) to recover high purity crystals of 98-99% as a final product. The overall yield of artemisinin is expected to reach 60% from the initial content of artemisinin in *A. annua* leaves. The spent mother liquor is guided for another row of crystallization with longer residence time. The recovered crude crystals are washed with cold ethanol to recover purer artemisinin and increase the final yield.

Conclusion

The inhibition of SARS-CoV-2 SProtein RBD with HCQ was successfully studied using molecular docking techniques. HCQ was found to selectively interact with the Lys353 hotspot binding pocket via the formation of an inclined tape over the binding site with the OH group of HCQ acting like a hook. Artemisinin class of compounds were also found to interact the same binding pocket. In addition, artemisinin & derived molecules showed extra mode of interaction with the Lys31 binding hotspot, although at slightly lower Vina score. Molecular dynamics studies confirmed that the formed complexes are able to interact and remain stable in the active site of their respective targets. These results demonstrate the likelihood of repurposing artemisinin as a less toxic substitute of HCQ to block the SProtein RBD of the virus from docking onto hACE2, while at the same time enhancing the immune system of the patient. More focus should be intended to study the *in-vivo* mode of action of artenimol as most artemisinin derivatives are converted to this compound once incorporated to the body.

Acknowledgements

The authors would like to acknowledge the support of the Directorate General of Scientific Research and Technological Development of the Ministry of High Education and Scientific Research in Algeria. We are thankful to Dr. Djamila Benrezkallah (Djillali Liabes University of Sidi Bel Abbes, Algeria) and Al-Farabi Cluster computer of the Ecole Nationale Polytechnique Oran – Maurice Audin for running the MD computations and insightful analysis of the molecular dynamics calculation.

Disclosure statement

No potential conflict of interest was reported by the author(s).

ORCID

Smain Chemat http://orcid.org/0000-0003-2123-9603

References

Boopathi, S., Poma, A. B., & Kolandaivel, P. (2020). Novel 2019 coronavirus structure, mechanism of action, antiviral drug promises and rule out against its treatment. *Journal of Biomolecular Structure and Dynamics*. https://doi.org/10.1080/07391102.2020.1758788

Chemat, S., Aissa, A., Boumechhour, A., Arous, O., & Ait-Amar, H. (2017). Extraction mechanism of ultrasound assisted extraction and its effect on higher yielding and purity of artemisinin crystals from *Artemisia annua* L. leaves. *Ultrasonics Sonochemistry*, *34*, 310–316. https://doi.org/10.1016/j.ultsonch.2016.05.046

Chemat, S., Boudjelal, S., Malki, I., & Lapkin, A. (2019). Biosynthesis of spathulenol and camphor stand as a competitive route to artemisinin production as revealed by a new chemometric convergence approach based on nine locations' field-grown *Artemisia annua* L. *Industrial Crops and Products*, *137*, 521–527. https://doi.org/10.1016/j.indcrop.2019.05.056

D'Alessandro, S., Scaccabarozzi, D., Signorini, L., Perego, F., Ilboudo, D. P., Ferrante, P., & Delbue, S. (2020). The use of antimalarial drugs against viral infection. *Microorganisms*, *8*(1), 85. https://doi.org/10.3390/microorganisms8010085

De Clercq, E. (2006). Potential antivirals and antiviral strategies against SARS coronavirus infections. *Expert Review of anti-Infective Therapy*, *4*(2), 291–302. https://doi.org/10.1586/14787210.4.2.291

Dietrich, J. A., Yoshikuni, Y., Fisher, K. J., Woolard, F. X., Ockey, D., McPhee, D. J., Renninger, N. S., Chang, M. C. Y., Baker, D., & Keasling, J. D. (2009). A novel semi-biosynthetic route for artemisinin production using engineered substrate-promiscuous P450(BM3). *ACS Chemical Biology*, *4*(4), 261–267. https://doi.org/10.1021/cb900006h

Dille, B. J., & Johnson, T. C. (1982). Inhibition of vesicular stomatitis virus glycoprotein expression by chloroquine. *Journal of General Virology*, *62*(1), 91–103. https://doi.org/10.1099/0022-1317-62-1-91

Gupta, M. K., Vemula, S., Donde, R., Gouda, G., Behera, L., & Vadde, R. (2020). In-silico approaches to detect inhibitors of the human severe acute respiratory syndrome coronavirus envelope protein ion channel. *Journal of Biomolecular Structure and Dynamics*. https://doi.org/10.1080/07391102.2020.1751300

Hale, V., Keasling, J. D., Renninge, N., & Diagana, T. T. (2007). Microbially derived artemisinin: A biotechnology solution to the global problem of access to affordable antimalarial drugs. *The American Journal of Tropical Medicine and Hygiene*, *77*(6 Suppl), 198–202. https://doi.org/10.4269/ajtmh.2007.77.198

Hasan, A., Paray, B. A., Hussain, A., Qadir, F. A., Attar, F., Aziz, F. A., Sharifi, M., Derakhshankhah, H., Rasti, B., Mehrabi, M., Shahpasand, K., Saboury, A. A., & Falahati, M. (2020). A review on the cleavage priming of the spike protein on coronavirus by angiotensin-converting enzyme-2 and furin. *Journal of Biomolecular Structure and Dynamics*. https://doi.org/10.1080/07391102.2020.1754293

He, R., Forman, M., Bryan, T., Mott, B. T., Venkatadri, R., Gary, H., Posner, G. H., & Arav-Boger, R. (2013). Unique and highly selective anticytomegalovirus activities of artemisinin-derived dimer diphenyl phosphate stem from combination of dimer unit and a diphenyl phosphate moiety. *Antimicrobial Agents and Chemotherapy*, *57*(9), 4208–4214. https://doi.org/10.1128/AAC.00893-13

Huter, M. J., Schmidt, A., Mestmäcker, F., Sixt, M., & Strube, J. (2018). Systematic and model-assisted process design for the extraction and purification of artemisinin from Artemisia annua L.—Part IV: Crystallization. *Processes*, *6*(10), 181. (https://doi.org/10.3390/pr6100181

Khan, S. A., Zia, K., Ashraf, S., Uddin, R., & Ul-Haq, Z. (2020). Identification of chymotrypsin-like protease inhibitors of SARS-CoV-2 via integrated

computational approach. *Journal of Biomolecular Structure and Dynamics*. https://doi.org/10.1080/07391102.2020.1751298

Lan, J., Ge, J., Yu, J., Shan, S., Zhou, H., Fan, S., Zhang, Q., Shi, X., Wang, Q., Zhang, L., & Wang, X. (2020). Structure of the SARS-CoV-2 spike receptor-binding domain bound to the ACE2 receptor. *Nature*, *581*(7807), 215–220. https://doi.org/10.1038/s41586-020-2180-5

Li, Q., Xie, L. H., Johnson, T. O., Si, Y., Haeberle, A. S., & Weina, P. J. (2007). Toxicity evaluation of artesunate and artelinate in Plasmodium berghei-infected and uninfected rats. *Transactions of the Royal Society of Tropical Medicine and Hygiene*, *101*(2), 104–112. https://doi.org/10.1016/j.trstmh.2006.04.010

Liu, J., Cao, R., Xu, M., Wang, X., Zhang, H., Hu, H., Li, Y., Hu, Z., Zhong, W., & Wang, M. (2020). Hydroxychloroquine, a less toxic derivative of chloroquine, is effective in inhibiting SARS-CoV-2 infection in vitro. *Cell Discovery*, *6*, 16. https://doi.org/10.1038/s41421-020-0156-0

Micholas, S., & Jeremy, C. (2020). Repurposing therapeutics for COVID-19: Supercomputer-based docking to the SARS-CoV-2 viral spike protein and viral spike protein-human ACE2 interface. *ChemRxiv*. https://doi.org/10.26434/chemrxiv.11871402.v4

Million, M., Lagier, J.-C., Gautret, P., Colson, P., Fournier, P.-E., Amrane, S., Hocquart, M., Mailhe, M., Esteves-Vieira, V., Doudier, B., Aubry, C., Correard, F., Giraud-Gatineau, A., Roussel, Y., Berenger, C., Cassir, N., Seng, P., Zandotti, C., Dhiver, C., … Raoult, D. (2020). Early treatment of COVID-19 patients with hydroxychloroquine and azithromycin: A retrospective analysis of 1061 cases in Marseille, France. *Travel Medicine and Infectious Disease*, *35*, 101738. https://doi.org/10.1016/j.tmaid.2020.101738

Muralidharan, N., Sakthivel, R., Velmurugan, D., & Gromiha, M. M. (2020). Computational studies of drug repurposing and synergism of lopinavir, oseltamivir and ritonavir binding with SARS-CoV-2 protease against COVID-19. *Journal of Biomolecular Structure and Dynamics*. https://doi.org/10.1080/07391102.2020.1752802

Pettersen, E. F., Goddard, T. D., Huang, C. C., Couch, G. S., Greenblatt, D. M., Meng, E. C., & Ferrin, T. E. (2004). UCSF Chimera-a visualization system for exploratory research and analysis. *Journal of Computational Chemistry*, *25*(13), 1605–1612. https://doi.org/10.1002/jcc.20084

Ramos, R. S., Macêdo, W. J. C., Costa, J. S., Da Silva, C. H. T. P., Rosa, J. M. C., Da Cruz, J. N., De Oliveira, M. S., De Aguiar Andrade, E. H., De Silva, R. B. L., Souto, R. N. P., & Santos, C. B. R. (2019). Potential inhibitors of the enzyme acetylcholinesterase and juvenile hormone with insecticidal activity: Study of the binding mode via docking and molecular dynamics simulations. *Journal of Biomolecular Structure and Dynamics*. https://doi.org/10.1080/07391102.2019.1688192

Romero, M. R., Efferth, T., Serrano, M. A., Castaño, B., Macias, R. I. R., Briz, O., & Marin, J. J. G. (2005). Effect of artemisinin/artesunate as inhibitors of hepatitis B virus production in an "in vitro" replicative system. *Antiviral Research*, *68*(2), 75–83. https://doi.org/10.1016/j.antiviral.2005.07.005

Samarth, S., & Kirk, M. G. (2020). Energetics based modeling of hydroxychloroquine and azithromycin binding to the SARS-CoV-2 spike (S)Protein - ACE2 Complex. *ChemRxiv*. https://doi.org/10.26434/chemrxiv.12015792.v2

Schrezenmeier, E., & Dörner, T. (2020). Mechanisms of action of hydroxychloroquine and chloroquine: Implications for rheumatology. *Nature Reviews. Rheumatology*, *16*(3), 155–166. https://doi.org/10.1038/s41584-020-0372-x

Shang, J., Ye, G., Shi, K., Wan, Y., Luo, C., Aihara, H., Geng, Q., Auerbach, A., & Li, F. (2020). Structural basis of receptor recognition by SARS-CoV-2. *Nature*, *581*(7807), 221–224. https://doi.org/10.1038/s41586-020-2179-y

Simmons, G., Reeves, J. D., Rennekamp, A. J., Amberg, S. M., Piefer, A. J., & Bates, P. (2004). Characterization of severe acute respiratory syndrome-associated coronavirus (SARS-CoV) spike glycoprotein-mediated viral entry. *Proceedings of the National Academy of Sciences of the United States of America*, *101*(12), 4240–4245. https://doi.org/10.1073/pnas.0306446101

Trott, O., & Olson, A. J. (2010). AutoDock Vina: Improving the speed and accuracy of docking with a new scoring function, efficient optimization and multithreading. *Journal of Computational Chemistry*, *31*(2), 455–461. https://doi.org/10.1002/jcc.21334

Vankadari, N., & Wilce, J. A. (2020). Emerging WuHan (COVID-19) coronavirus: Glycan shield and structure prediction of spike glycoprotein and its interaction with human CD26. *Emerging Microbes & Infections*, *9*(1), 601–604. https://doi.org/10.1080/22221751.2020.1739565

Vincent, M. J., Bergeron, E., Benjannet, S., Erickson, B. R., Rollin, P. E., Ksiazek, T. G., Seidah, N. G., & Nichol, S. T. (2005). Chloroquine is a potent inhibitor of SARS coronavirus infection and spread. *Virology Journal*, *2*, 69. https://doi.org/10.1186/1743-422X-2-69

Wang, M., Cao, R., Zhang, L., Yang, X., Liu, J., Xu, M., Shi, Z., Hu, Z., Zhong, W., & Xiao, G. (2020). Remdesivir and chloroquine effectively inhibit the recently emerged novel coronavirus (2019-nCoV) in vitro. *Cell Research*, *30*(3), 269–271. https://doi.org/10.1038/s41422-020-0282-0

Weniger, H. (1979). Review of side effects and toxicity of chloroquine. *The Bulletin of the World Health Organization*, *79*, 906.

Woodrow, C. J., Haynes, R. K., & Krishna, S. (2005). Artemisinins. *Postgraduate Medical Journal*, *81*(952), 71–78. https://doi.org/10.1136/pgmj.2004.028399

Yan, R., Zhang, Y., Li, Y., Xia, L., Guo, Y., & Zhou, Q. (2020). Structural basis for the recognition of SARS-CoV-2 by full-length human ACE2. *Science (New York, N.Y.).)*, *367*(6485), 1444–1448. https://doi.org/10.1126/science.abb2762

Yang, Z. Y., Huang, Y., Ganesh, L., Leung, K., Kong, W. P., Schwartz, O., Subbarao, K., & Nabel, G. J. (2004). pH-dependent entry of severe acute respiratory syndrome coronavirus is mediated by the spike glycoprotein and enhanced by dendritic cell transfer through DC-SIGN. *Journal of Virology*, *78*(11), 5642–5650. https://doi.org/10.1128/JVI.78.11.5642-5650.2004

Yao, W., Wang, F., & Wang, H. (2016). Immunomodulation of artemisinin and its derivatives. *Science Bulletin*, *61*(18), 1399–1406. https://doi.org/10.1007/s11434-016-1105-z

Zhou, P., Yang, X., Wang, X., Hu, B., Zhang, L., Zhang, W., Si, H. R., Zhu, Y., Li, B., Huang, C. L., Chen, H. D., Chen, J., Luo, Y., Guo, H., Jiang, R. D., Liu, M. Q., Chen, Y., Shen, X. R., Wang, X., … Shi, Z. L. (2020). A pneumonia outbreak associated with a new coronavirus of probable bat origin. *Nature*, *579*(7798), 270–273. https://doi.org/10.1038/s41586-020-2012-7